Molecular Reorganization of Paired Assemblies of T-Shaped Rod−Coil Amphiphilic Molecule at the Air−Water Interface

Libin Liu,[†] Kyung-Soo Moon,[†] Ray Gunawidjaja,[‡] Eunji Lee,[†] Vladimir V. Tsukruk,*[,‡] and Myongsoo Lee*[,†]

Center for Supramolecular Nano-Assembly, Department of Chemistry, Yonsei University, Seoul 120-749, Korea, and School of Materials Science and Engineering, Georgia Institute of Technology, Atlanta, Georgia 30332

Received November 23, 2007. In Final Form: January 10, 2008

A T-shaped aromatic amphiphilic molecule based on linear oligo(ethylene oxide) was synthesized. We suggest that its peculiar interfacial behavior at the air−water interface and the structure of the Langmuir−Blodgett monolayer are associated with its peculiar T-shape and competing steric and amphiphilic interactions at different surface pressures. At low surface pressure, uniform and smooth monolayers were formed. Upon compression, the molecular reorganization from spherical to cylindrical transformation occurred, as caused by the submerging of the oligo(ethylene oxide) chains, providing for efficient $\pi-\pi$ interactions of the central core. At the highest surface pressure, the monolayer collapses into bilayer domains, following a bicontinuous network formation which tends to transform into a perforated film. The unique shape of T-like rigid aromatic cores makes their structural reorganization very peculiar with *paired, dimerlike* molecular packing dominating in gas and solid states. This paired aggregation is so strong that it is preserved in the course of flipping and formation of vertically oriented backbones.

Introduction

Rod−coil molecules composed of a rigid rod and a flexible coil block are a novel type of block copolymer with a unique microstructural organization held together by noncovalent forces, including hydrophobic and hydrophilic effects, electrostatic interaction, and hydrogen bonding.[1] The fabrication of self-assembled architectures with well-defined organization at the surfaces and interfaces controlled by chemical architecture and interfacial interactions is a long-standing topic in surface and material science.[2,3] Rod−coil molecules as a typical self-assembly system have been widely investigated in solution and a solid state, where they are capable of self-assembling into various nanostructures such as lamellar, cylindrical, or spherical.[4−6] However, investigations concerning thin-film structures of rod−coil molecules on a solid support are rarely found.[7,8] Poly(ethy1ene oxide) (PEO), a common hydrophilic flexible block of these molecules, is known to form stable spread films at the air−water interface due to the cooperative interfacial contacts, even if the monomer segments themselves are only mildly amphiphilic.[9] Amphiphilic diblock copolymers have been shown to self-assemble into well-defined nanoscale structures in both two- and three-dimensions.[10,11] For amphiphilic rod−coil molecules, water-soluble flexible PEO tails can submerge in water subphase during compression, thus forming a thin polymer layer enriched with water molecules beneath the hydrophobic rod blocks and changing the effective composition at the air−water interface, giving rise to a variety of interfacial structures in linear and star block copolymers.[7b,8] A variable effective composition may lead to the significant conformational changes, surface aggregation, or the morphological transition of the aggregates depending upon external conditions such as surface pressure, solvent evaporation, or dewetting behavior.[12]

In our previous work, we have synthesized T-shaped aromatic amphiphiles based on oligo(ethylene oxide) dendrons and demonstrated the formation of thermoresponsive nanoscale fibrils due to self-assembly of the molecules.[13] In aqueous solution, they formed fibrillar morphology whose aspect ratio varies with the crowding of the hydrophilic chains. Greater aspect ratio was observed for the linear oligo(ethylene oxide) and lower aspect

* To whom correspondence should be addressed. E-mail: mslee@yonsei.ac.kr (M.L.), Vladimir@mse.gatech.edu (V.V.T.).

[†] Yonsei University.

[‡] Georgia Institute of Technology.

(1) Whitesides, G. M.; Mathias, J. P.; Seto, C. T. *Science* **1991**, *254*, 1312.

(2) Ulman, A. *An Introduction to Ultrathin Organic Film: From Langmuir-Blodgett to Self-Assembly*; Academic Press: Boston, MA, 1991.

(3) (a) Tsukruk, V. V. *Prog. Polym. Sci.* **1997**, *22*, 247. (b) Luzinov, I.; Minko, S.; Tsukruk, V. V. *Prog. Polym. Sci.* **2004**, *29*, 635. (c) Tsukruk, V. V. *Adv. Mater.* **2001**, *13*, 95.

(4) Jenekhe, S. A.; Chen, X. L. *Science* **1999**, *283*, 372.

(5) (a) Lee, M.; Cho, B.-K.; Zin, W.-C. *Chem. Rev.* **2001**, *101*, 3869. (b) Ryu, J.-H.; Oh, N.-K.; Zin, W.-C.; Lee, M. *J. Am. Chem. Soc.* **2004**, *126*, 3551. (c) Lee, M.; Park, M.-H.; Oh, N.-K.; Zin, W.-C.; Jung, H.-T.; Yoon, D.-K. *Angew. Chem., Int. Ed.* **2004**, *43*, 6465. (d) Kim, J.-K.; Hong, M.-K.; Ahn, J.-H.; Lee, M. *Angew. Chem., Int. Ed.* **2005**, *44*, 328. (e) Kim, J.-K.; Lee, E.; Huang, Z.; Lee, M. *J. Am. Chem. Soc.* **2006**, *128*, 14022. (f) Kim, J.-K.; Lee, E.; Jeong, Y.-H.; Lee, J.-K.; Zin, W.-C.; Lee, M. *J. Am. Chem. Soc.* **2007**, *129*, 6082.

(6) Klok, H.-A.; Lecommandoux, S. *Adv. Mater.* **2001**, *13*, 1217.

(7) (a) Li, H. B.; Liu, Q. T.; Xu, M.; Bu, W. F.; Lin, X. K.; Wu, L. X.; Shen, J. C. *J. Phys. Chem. B* **2005**, *109*, 2855. (b) Zhang, J.; Cao, H. Q.; Wan, X. H.; Zhou, Q. F. *Langmuir* **2006**, *22*, 6587.

(8) (a) Tsukruk, V. V.; Genson, K.; Peleshanko, S.; Markutsya, S.; Lee, M.; Yoo, Y.-S. *Langmuir* **2003**, *19*, 495. (b) Holzmueller, J.; Genson, K. L.; Park, Y.; Yoo, Y.-S.; Park, M.-H.; Lee, M.; Tsukruk, V. V. *Langumir* **2005**, *21*, 6392.

(9) (a) Shuler, R. L.; Zisman, W. A. *J. Phys. Chem.* **1970**, *74*, 1523. (b) Kawaguchi, M.; Komatsu, S.; Matsuzumi, M.; Takahashi, A. *J. Colloid Interface Sci.* **1984**, *102*, 356. (c) Sauer, B. B.; Kawaguchi, M.; Yu, H. *Macromolecules* **1987**, *20*, 2732. (d) Kuzmenka, D. J.; Granick, S. *Macromolecules* **1988**, *21*, 779. (e) Kuzmenka, D. J.; Granick, S. *Polym. Commun.* **1988**, *29*, 64.

(10) (a) Zhu, J.; Eisenberg, A.; Lennox, R. B. *Langmuir* **1991**, *7*, 1579. (b) Zhu, J.; Eisenberg, A.; Lennox, R. B. *J. Am. Chem. Soc.* **1991**, *113*, 5583. (c) Zhu, J.; Eisenberg, A.; Lennox, R. B. *Macromolecules* **1992**, *25*, 6547. (d) Zhu, J.; Eisenberg, A.; Lennox, R. B. *Macromolecules* **1992**, *25*, 6556. (e) Zhu, J.; Eisenberg, A.; Lennox, R. B. *J. Phys. Chem.* **1992**, *96*, 4727.

(11) (a) Cox, J. K.; Eisenberg, A.; Lennox, R. B. *Curr. Opin. Colloid Interface Sci.* **1999**, *4*, 52. (b) Cox, J. K.; Yu, K.; Eisenberg, A.; Lennox, R. B. *Phys. Chem. Chem. Phys.* **1999**, *18*, 4417.

(12) (a) Lee, M.; Kim, J.-W.; Peleshanko, S.; Larson, K.; Yoo. Y.-S.; Vaknin, D.; Markutsya, S.; Tsukruk, V. V. *J. Am. Chem. Soc.* **2002**, *124*, 9121. (b) Zhai, X.; Peleshanko, S.; Klimenko, N. S.; Genson, K. L.; Vaknin, D.; Vortman, M. Ya.; Shevchenko, V. V.; Tsukruk, V. V. *Macromolecules* **2003**, *36*, 3101. (c) Genson, K. L.; Holzmueller, J.; Ornatska, M.; Yoo, Y.-S.; Park, M.-H.; Lee, M.; Tsukruk, V. V. *Nano Lett.* **2006**, *6*, 435.

(13) Moon, K.-S.; Kim, H. J.; Lee, E.; Lee, M. *Angew. Chem., Int. Ed.* **2007**, *46*, 6807.

10.1021/la703660v CCC: $40.75
Published on Web 03/01/2008

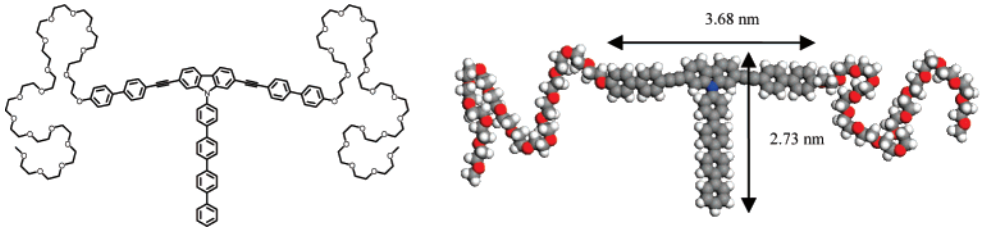

Figure 1. Chemical structure and corresponding molecular model of the T-shaped molecule.

ratio for branched oligo(ethylene oxide) as controlled by the steric hindrances at the branching points.

Herein, we have synthesized a different type of T-shaped aromatic amphiphile based on linear oligo(ethylene oxide) and observed its peculiar interfacial behavior (Figure 1). It is conceivable that crowding of aromatic rods at the air−water interface will lead to the orientation of rods, which will affect the microstructure of the Langmuir−Blodgett (LB) monolayer film. Moreover, it is expected that the variable effective compositions induced by the conformation changes of PEO under compression will tend toward structural reorganization of the T-shaped core and lead to a morphological transition.

Experimental Section

Synthesis of T-Shaped Molecule. The synthesis procedure of the T-shaped molecule was similar to that described in our previous work.[13] It has a molecular weight of 2294 Da with 64% weight content of hydrophilic poly(ethylene glycol). Poly(ethylene glycol) (M_W = 750 Da) from Aldrich was used as received. ^{1}H and ^{13}C NMR spectra were recorded from $CDCl_3$ and DMSO solutions on a Bruker AM 250 spectrometer and Bruker AVANCE 400 spectrometer. The purity of the products was checked by thin layer chromatography (TLC; Merck, silica gel 60). Microanalyses were performed with a Perkin-Elmer 240 elemental analyzer at Organic Chemistry Research Center, Sogang University. MALDI TOF-MS was performed on a Perceptive Biosystems Voyager-DE STR using a 2,5-dihydroxybenzoic acid matrix. Preparative high-performance liquid chromatography (prep HPLC) was performed at room temperature using a 20 mm × 600 mm polystyrene column on a Japan Analytical Industry Model LC-908 recycling prep HPLC system, equipped with UV detector 310 and RI detector RI-5. Yield: 50%. ^{1}H NMR (250 MHz, $CDCl_3$, ppm): δ = 8.12 (d, 2Ar-*H*, *J* = 8.0 Hz), 7.94 (d, 2Ar-*H*, *J* = 8.4 Hz), 7.82−7.36 (m, 31Ar-*H*), 7.01 (d, 4Ar-*H*, *J* = 8.8 Hz), 4.17 (t, 4H; Ar−OC*H*$_2$, *J* = 5.1 Hz), 3.87 (t, 4H; Ar−OCH$_2$C*H*$_2$, *J* = 5.1 Hz), 3.74−3.53 (m, 120H; OC*H*$_2$), 3.37 (s, 6H; OC*H*$_3$). ^{13}C NMR (100 MHz, $CDCl_3$, ppm): δ = 159.0, 141.3, 140.6, 140.4, 140.0, 139.4, 139.1, 136.1, 132.0, 128.9, 128.7, 128.1, 127.6, 127.4, 127.1, 126.5, 124.1, 123.1, 121.5, 121.1, 120.5, 114.9, 113.1, 91.1, 89.8, 76.8, 71.9, 70.8, 70.6, 70.5, 69.7, 67.5, 59.0. MALDI-TOF-MS: *m*/*z* 2315.18 ([M + Na]$^+$), calcd 2315.23. Anal. Calcd for $C_{146}H_{205}NO_{42}$: C, 68.07; H, 7.60; N, 0.61. Found: C, 68.08; H, 7.68; N, 0.58.

Monolayer Fabrication. Langmuir isotherms at the air−water interface and LB depositions onto a silicon substrate were conducted at room temperature using a KSV 2000 LB minitrough according to the usual procedure.[14] A 40−120 μL volume of dilute polymer solution (concentration less than 0.5 mg/mL) in chloroform (HPLC grade) was deposited in 5−10 drops uniformly distributed onto the water surface (Nanopure, 18.2 MΩ cm) and left to evaporate and spread evenly over a period of 30 min. The limiting cross-sectional area (A_0) was determined at the steep rise in the surface pressure related to the formation of condensed monolayer. For AFM measurement, the monolayer LB films of the T-PEO molecule were transferred at a rate of 2 mm/min onto silicon wafers at various surface pressures by the upstroke mode of the vertical dipping method. The typical transfer ratio is in the range of 0.8 and 1.0, which suggests a good film quality, as expected for the significant hydrophilic content in the form of PEO chain, i.e., 64.2% weight content deposited on "piranha"-treated Si/SiO_2 surface.[15] For UV−vis and FTIR spectral measurements, the floating films were transferred onto quartz and ZnSe solid supports at selected surface pressure by the horizontal Langmuir−Schaefer method and by a certain number of depositions.

Spin-coated films were fabricated on a PM101DT-R485 spinner (Headway Research, Inc., Garland, TX) at 1000 rpm for 15 s at room temperature. Highly polished [100] silicon wafers (Semiconductor Processing Co.) were cut into rectangular pieces (2 × 2 cm^2) and sonicated in Nanopure water for 10 min to remove silicon dust. The wafers were then chemically treated with piranha solution (30% concentrated hydrogen peroxide, 70% concentrated sulfuric acid) (**Caution:** *hazardous solution!*) for 1 h to strip off any organic contaminants that cling onto the silicon oxide surface, while at the same time oxidizes/hydroxylates the surface.[16] Subsequent rinsing with Nanopure water results in a fresh silicon oxide layer with a high concentration of silanol groups. Its thickness is about 1.2 nm, as determined by ellipsometry, and its surface microroughness is below 0.1 nm within the 1 × 1 μm^2 surface area.

Monolayer Characterization. The effective thickness of the LB monolayers was measured with an M-2000 U Spectroscopic Ellipsometer (J. A. Woolam Co.). Contact angle was measured by the sessile drop method on a custom-built instrument that combines a microscope and digital camera. UV−vis measurements of the films were performed at room temperature using a UV-1650PC spectrophotometer. FTIR measurements were recorded on Equinox 55 FT-IR spectrophotometer with an average of several hundred scans. The LB monolayers on the silicon substrates were studied with a Nanoscope IIIa Multimode AFM. Scans were performed in the "light" tapping mode, in accordance with the usual procedure adapted in our laboratory.[17] An amplitude ratio of 0.95 and higher was employed to avoid monolayer damage.[18] AFM characterization of the deposited LB films was done after drying in a desiccator for 24 h. The AFM scans were conducted at 0.5−2 Hz scanning rate for surface areas range from 20 × 20 μm^2 to 250 × 250 nm^2 and for several randomly selected locations with at least 40 different images collected for each specimen. The domain topography and the surface area coverage were calculated from height histograms using the bearing analysis.[19] The tip radius was measured independently using tethered gold nanoparticles as a standard reference, and only the sharpest tips were selected for high-resolution scanning. The AFM tip radii were between 20 and 35 nm, and the spring constants of these cantilevers were in the range of 40−60 N/m.

Results and Discussion

Monolayer Behavior at the Air−Water Interface. Surface−area isotherms of the T-shaped molecule at the air−water interface obtained at two different initial concentrations are represented in Figure 2. The reversibility of the Langmuir monolayers was

(14) (a) Larson, K.; Vaknin, D.; Villavicencio, O.; McGrath, D.; Tsukruk, V. V. *J. Phys. Chem. B* **2002**, *106*, 7246. (b) Sidorenko, A.; Houphouet-Boigny, C.; Villavicencio, O.; McGrath, D. V.; Tsukruk, V. V. *Thin Solid Films* **2002**, *410*, 147.

(15) Chen, C.-W.; Liu, T.-J. *J. Colloid Interface Sci.* **2006**, *298*, 298.

(16) Szunerits, S.; Boukherroub, R. *Langmuir* **2006**, *22*, 1660.

(17) (a) Tsukruk, V. V.; Reneker, D. H. *Polymer* **1995**, *36*, 1791. (b) Tsukruk, V. V. *Rubber Chem. Technol.* **1997**, *70*, 430.

(18) Magonov, S. N.; Elings, V.; Whangbo, M. H. *Surf. Sci.* **1997**, *375*, L385.

(19) Magonov, S. N. *Surface Analysis with STM and AFM: Experiment and Theoretical Aspects of Image Analysis*; VCH: New York, 1996.

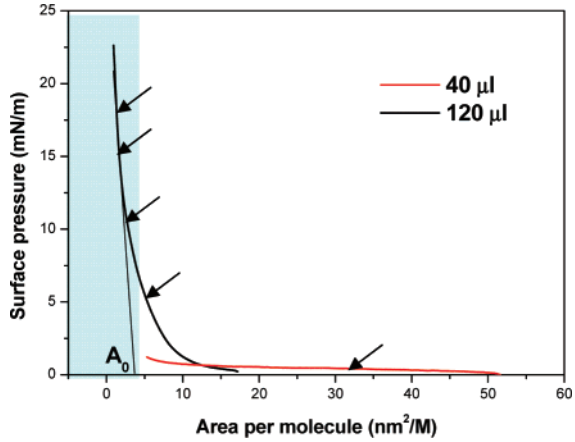

Figure 2. Surface pressure−area ($\pi-A$) isotherms of the T-shaped molecule using different volumes. Arrows mark LB deposition pressures and a shadow indicates the solid state of the monolayer.

examined by repeating cycles of compression and expansion within the low pressure (<5 mN/m) regime (not shown). The complete pressure−area isotherm for the molecule by using low volume solution was technically difficult to obtain within one run due to the limited compression ratio of the LB trough. A gradual increase in surface pressure up to 1.5 mN/m under compression observed for larger initial concentration is due to the gradual submerging of the PEO segments into the water subphase from the initial flattened conformation at very low surface pressure, as was discussed in literature (Figure 2).[20] The steep increase in the surface pressure at area/molecule below 5 nm^2 is due to the crowding of aromatic rods upon compression after the PEO chains became completely submerged into the water subphase, a very common behavior for starlike polymers.[21]

As known, the Langmuir isotherms of diblock molecules containing the large PEO block usually possess a plateau at the surface pressure below 10 mN/m, which corresponds to a two-dimensional to three-dimensional (2D-to-3D) phase transition of the PEO block.[22,23] In our present case, the isotherm of the T-shaped molecule does not present such a plateau, which should be caused by the much smaller PEO block content and short PEO chains. The limiting cross-sectional surface area/molecule (A_0), calculated by the extrapolation of the steep rise in the surface pressure to a zero level, is 3.62 nm^2. The theoretical surface area occupied by the hydrophobic rod block was calculated to be about 3.97 nm^2, similar to the limiting area, indicating that the aromatic rod adopts a face-on orientation rather than a titled orientation, which confirms the critical role of the aromatic core in the surface behavior of the Langmuir monolayer at high surface pressure (Figure 1).

The effective thickness of the LB monolayer deposited at the cross-sectional area of 33 nm^2 is very small, 0.39 nm (Table 1), confirming the flat, face-on arrangement of the rigid cores tethered by the spread PEO chains at the air−water interface (Figure 3, Table 1). At a high surface area (area/molecule of 5.58 nm^2) closer to but still higher than the limiting cross-sectional area of the molecule (3.62 nm^2), the effective thickness increased to 0.46 nm (Table 1).

Table 1. Monolayer Thickness and Domain Heights at Different Surface Pressure

P (mN/m)	area/molec[a] (nm^2)	domain height[b] (nm)	calcd height[c] (nm)	ellipsometry (nm)	contact angle (deg)
0.5	33.00	0.61	0.40	0.39	25 ± 2
5	5.58	0.85	0.51	0.46	32 ± 2
10	2.85	4.20	0.93	0.86	33 ± 2
15	1.56	4.48	2.53	2.65	35 ± 2
18	1.25	4.70	4.27	4.42	38 ± 2

[a] Area/molecule was determined by $\pi-A$ isotherm. [b] Domain height was obtained by AFM cross-sectional analysis. [c] The sum of PEO thickness and, if it exists, domain height.

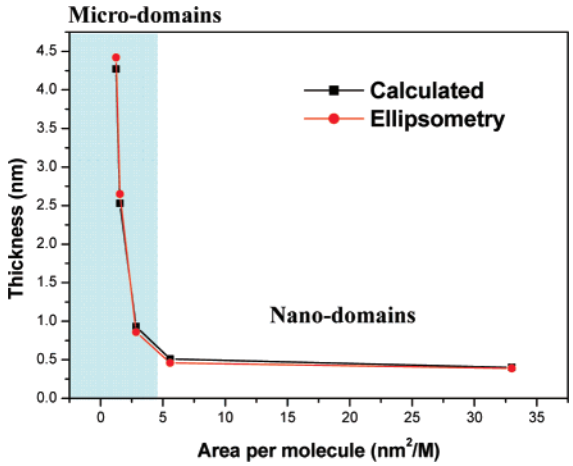

Figure 3. Calculated and measured monolayer thicknesses with decreasing area/molecule.

Further increasing the surface pressure up to 10 mN/m, below the limiting cross-sectional area (3.62 nm^2), resulted in a sharp a 2-fold increase in film thickness, which reaches 0.86 nm (Table 1). Further increase in the effective thickness at even higher surface pressure is attributable to the multilayer formation upon complete monolayer collapse (Table 1). The effective thickness measured by ellipsometry closely resembles the calculated thickness as based on the area/molecule and domain heights, such that for low surface pressure, P = 0.5 and 5 mN/m, we assumed that the T-shaped core is horizontally aligned and therefore the overall height is due to the hydrophilic PEO chains in its bulk state. The thickness of PEO domains, H_A, at any point on the Langmuir isotherm is calculated as the volume/molecule of bulk PEO divided by the area occupied by the molecule at that point. The volume/molecule of bulk PEO is calculated as $M_n/(\rho N_A)$, where M_n is the molecular weight of PEO, ρ is the bulk density of PEO,[24] and N_A is Avogadro's number. At high surface pressure, the effective thickness of the hydrophobic and hydrophilic domain mixture is calculated as $A_cH_B + (1 - A_c)H_A$, where A_c is the area coverage of hydrophobic domains, H_A is the height of the hydrophilic domain, and H_B is the height of the hydrophobic domain. Both the area coverage, A_c, and average hydrophobic domain heights, H_B, could be determined from AFM topography. The effective thickness is the sum of hydrophobic domain and hydrophilic domain, calculated over several 2 × 2 μm^2 areas.

LB Monolayers on a Solid Support. The surface properties of the deposited LB monolayers were first tested by analyzing the water contact angle. The monolayers deposited at low surface pressure exhibited low to moderate hydrophobic character (contact

(20) Sauer, B. B.; Yu, H. *Macromolecules* **1989**, *22*, 786.
(21) Genson, K. L.; Hoffman, J.; Teng, J.; Zubarev, E. R.; Vaknin, D.; Tsukruk, V. V. *Langmuir* **2004**, *20*, 9044.
(22) Bijsterbosch, H. D.; de Haan, V. O.; de Graaf, A. W.; Mellma, M.; Leemakers, F. A. M.; Cohen Stuart, M. A.; van Well, A. A. *Langmuir* **1995**, *11*, 4467.
(23) Gonçalves da Silva, A. M.; Simoes Gamboa, A. L.; Martinho, J. M. G. *Langumir* **1998**, *14*, 5327.
(24) Brandrup, J.; Immergut, E. H.; Grulke, E. A., Eds. *Polymer Handbook*, 4th ed; John Wiley & Sons: New York, 1999.

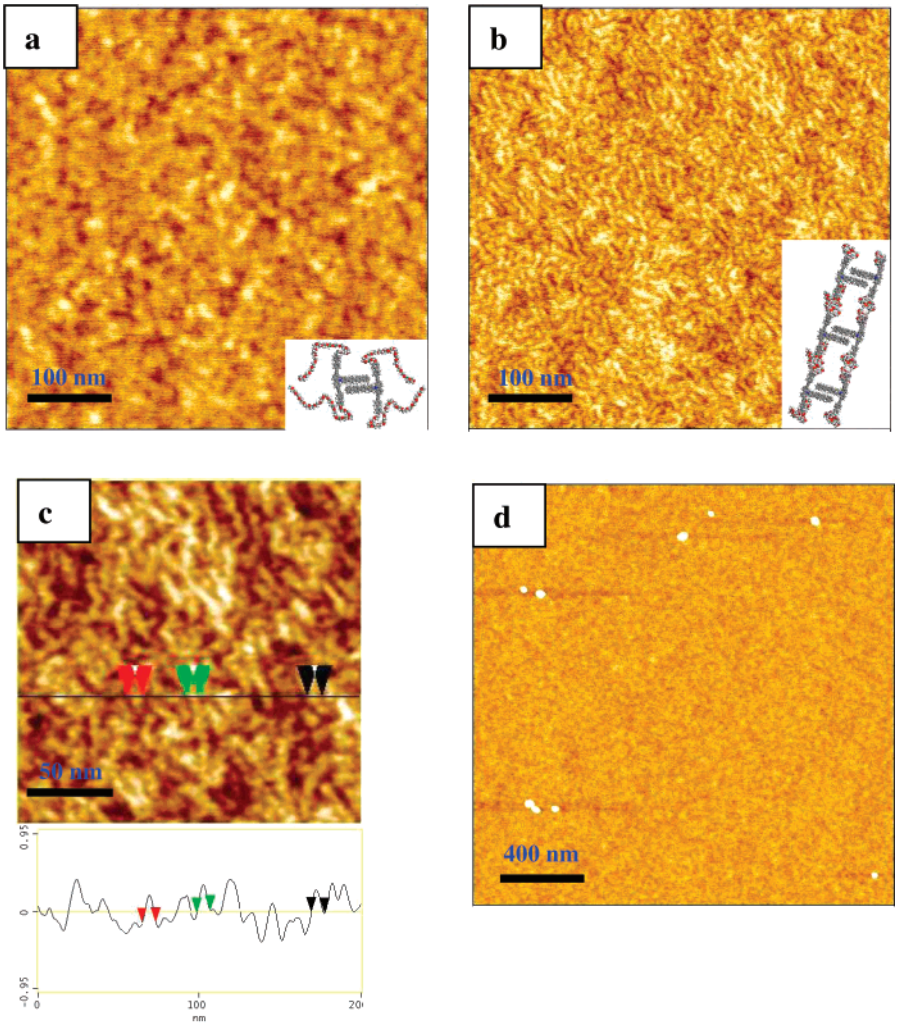

Figure 4. Topographical AFM images of T-shaped molecule at (a) low, $\pi = 0.5$ mN/m, and (b−d) intermediate, $\pi = 5$ mN/m, surface pressures. (c) Higher-resolution topographical image at $\pi = 5$ mN/m. (d) A lower magnification image at $\pi = 5$ mN/m. The *Z*-range is 3 nm for all images. Proposed molecular models are inserted in parts a and b, respectively.

angle in the range of 25°−32°), indicating a mixed surface composition (a contact angle of 80°−120° is expected for surface composed of phenyl rings and below 10° for dry PEO surface). Contact angle measurements revealed a slightly increasing hydrophobicity for the denser monolayer, which can be associated with greater exposure of hydrophobic core fragments and some screening of the PEO chains (Table 1).

AFM images demonstrate LB monolayers deposited at low surface pressure as showing smooth and uniform surface morphology on a microscopic scale (5−20 μm across). Higher magnification scans revealed a variety of surface morphologies associated with nanodomain organization (Figure 4). At very low surface pressure, $\pi = 0.5$ mN/m, irregular spherical morphologies are barely seen at the highest magnification. The low cross-sectional area of the spherical domains contradicts a tilted orientation of the rod core and favors a face-on orientation. At this state, PEO spreads on the water surface to form the shell and the rods form the core due to $\pi-\pi$ interaction. By considering the extended molecular lengths to be about 8 nm, as determined from the molecular models, we suggest that the diameter of the spherical domains visible on high-resolution AFM images at very low pressure ("gas state") corresponds to one molecular length. Thus, the proposed molecular model of isolated symmetrical domains with T-shaped cores surrounded by coiled PEO chains which fits to the lateral dimensions, the thickness of monolayers, and the area/molecule is shown in Figure 4a (inset). Some holes in the film correspond to the nanoscopic voids caused by defects between the paired and individual randomly oriented molecules.

Upon further increase in surface pressures to $\pi = 5$ mN/m (onset of solid monolayer formation), the monolayer remains relatively smooth, as seen from a larger scan area with occasional domains indicating localized bilayers formation (Figure 4d). At this pressure, the individual spheres transformed into long, slightly curved cylinders with aspect ratio reaching 5−10 (Figure 4b). Figure 4c shows the cross-sectional analysis of the corresponding high-resolution image that was used to evaluate the diameter of the cylinder to be about 5.5 nm (estimated taking into account tip dilation) and their length within 20−70 nm. Considering that, at this pressure, PEO chains are partly immersed into water and form the brush configuration,[22] the aromatic-rod will be more exposed at the air−water interface and form more densely packed structures. These structures involve paired packing of T-shaped cores with correlation along main axes providing for enhanced $\pi-\pi$ interaction and resulting in long cylindrical-like shapes of these aggregated structures (Figure 4b, inset). The diameters of these cylinders are smaller than those of initial spherical nanodomains formed at low surface pressure due to a decrease of PEO corona around the aromatic rod core at the water surface. On the basis of the length of the cylinder, each cylinder contains approximately 10−30 paired T-shaped molecules.

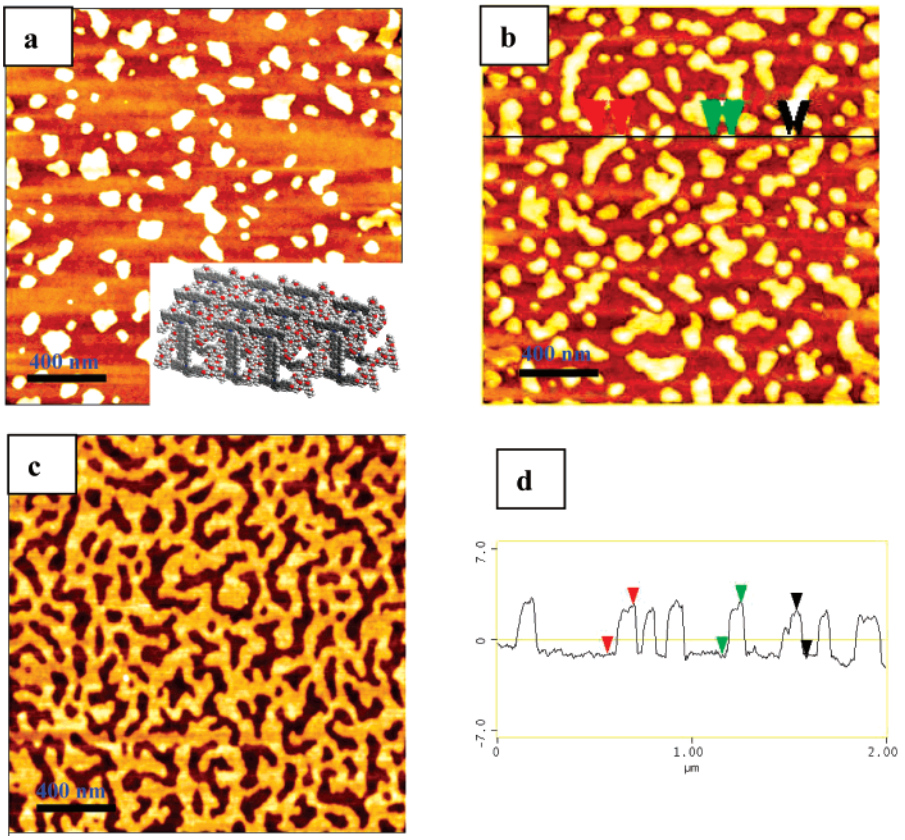

Figure 5. AFM images of LB monolayers from a T-shaped molecule at high surface pressure: (a) $\pi = 10$ mN/m, (b) $\pi = 15$ mN/m, (c) $\pi = 18$ mN/m, and (d) corresponding cross-section. The Z-range is 7 nm for all images.

Significant change in surface morphology accompanied with a notable increase in thickness was observed at even higher surface pressure, near monolayer collapse (Table 1, Figure 3). The films deposited at an area smaller than the limiting cross-sectional area of 3.62 nm^2 show the formation of randomly dispersed microdomains topping the smooth monolayer beneath (Figure 5). The distance between the irregular-shaped microdomains decreased to merge into greater islands and eventually into bicontinuous network morphologies as the surface pressure progressed. However, the heights stayed approximately constant (from 4.2 to 4.7 nm) after initial steep increase. This domain height corresponds to paired molecules adopting vertical conformation on the water surface, i.e., apparent bilayer formation expected for the precollapsed state (Figure 5a). Obviously, continuous compression reduces the area available for molecules and leads to complete dissolution of the flexible PEO chains into water and further to reorientation of T-shaped cores to a vertical position to accommodate the greatly reduced surface area.

To further confirm the structural change of the transferred film caused by the $\pi-\pi$ stacking interaction of the aromatic core and the conformational change of the PEO unit, UV−vis spectra and FTIR spectra were performed. Figure 6a shows the UV−vis spectra of the T-PEO molecule in both solution and LB films. The UV−vis spectrum of T-PEO in solution exhibits an absorption band at 299 nm and a broadened band centered around at 362 nm. In the LB films deposited at both low and high surface pressure, the band at lower energy shows a blue shift in comparison with the solution. In addition, comparing the spectrum of the film deposited at 18 mN/m with that at 0.5 mN/m, a further blue shift was observed. This blue shift of the absorption spectra in the LB films might be ascribed to the $\pi-\pi$ stacking of the aromatic rings, where they were arranged in a face-to-face way to form H-aggregate structures in LB films.[25] This is in agreement of the AFM images, where the aromatic rings are suggested to have a face-on arrangement.

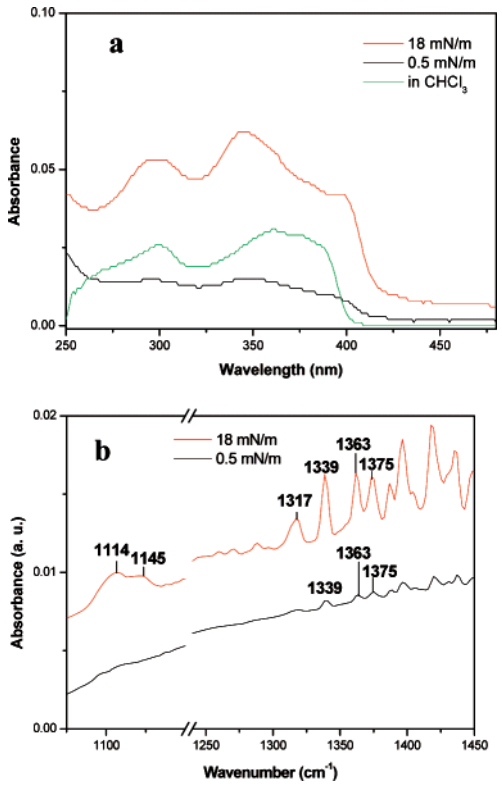

Figure 6. UV−vis spectra (a) and FTIR spectra (b) of 15-layer LB films of T-PEO molecule deposited on quartz and ZnSe slides, respectively.

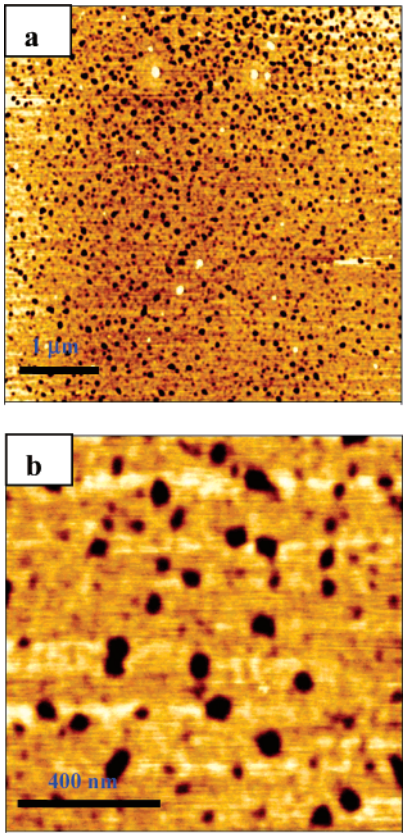

Figure 7. AFM images of spin-coated film at silicon substrate: (a) 5×5 μm^2 scan (topography), z range 10 nm; (b) 1×1 μm^2 scan (topography), z range 7 nm.

Figure 6b depicts the spectral region in which PEO conformation changes.[26] In contrast to the films deposited at low surface pressure of 0.5 mN/m, the film deposited at high surface pressure shows a different degree of variation in its molecular conformation. The spectrum of the film deposited at high surface pressure exhibits a shoulder at 1114 and 1145 cm^{-1} on the low-frequency side of the C−O−C-stretch band, which is characteristic for the crystalline phase of PEO.[27] The band at 1317 cm^{-1} in the film deposited at high surface pressure, which is barely observed in the spectra of the film deposited at low surface pressure, might be attributed to coupled CH_2-CH_2-wagging modes. This may be due to the film domains with a crystalline phase coexisted with an amorphous PEO phase at high surface pressure.[28]

This type of molecular packing is also characteristic for dense, ultrathin spin-cast films of T-shaped material (Figure 7). These films show the formation of more densely packed domains with pinhole defects caused by fast solvent evaporation. The domain height in these films is about 5.0 nm, similar to the height of domains with vertical packing of paired molecules formed at high Langmuir monolayer compression (Figure 5).

General Discussion and Conclusions

The mechanism of surface aggregates formation can be unambiguously interpreted by considering the $\pi-A$ isotherms and the surface morphologies as was demonstrated above. Overall, here we can distinguish and select one out of three of the most common mechanisms of the formation of the block copolymer surface aggregates: (1) deposition of the "preformed" micelles in solution, (2) compression-induced surface aggregation, and (3) spontaneous surface aggregation at the onset of deposition of polymer solution.[29] Since no micellar aggregates were present in the spreading solution at very low concentration (spreading solvent is chloroform), as confirmed by dynamic light scattering measurements,[29] we can preclude the possibility of deposition of the micelles from solution. Thus, we can conclude that spherical nanoaggregates observed in the gas state areas most likely to be spontaneously formed aggregates, which occur upon deposition of the polymer solution and the evaporation of the solvent.

Complex morphological transitions occur for these T-shaped molecules upon increasing surface pressure. Therefore, the compression-induced aggregation of different types following the initial assembly is another mechanism of surface organization caused by decreasing surface area available for molecules and the PEO surface behavior. At low surface pressure, spherical aggregates adopt the "starfish" conformation with the PEO corona absorbed at the interface.[20] Upon compression, the PEO coronas of surface aggregates begin to interact with each other, which gives rise to an increase of surface pressure in the course of formation of dense, solid monolayer. The dissolution of the PEO coronas into the water subphase begins at the same time the morphology changes from spheres to cylinders.[20] As the surface pressure increased from 0.5 to 5 mN/m, the compression ratio of PEO decreased from 61% to 4%, and the effective contents of the aromatic rod (W_{aromatic}'%) increased from 48 to 93 wt %.[30] This indicates that most of the PEO chains are submerged in water at a surface pressure of 5 mN/m. This reorganization can be related to the folding of the flexible tails and their dehydration due to expelling associated water molecules from densely packed areas beneath the air−water interface.[31] In this state, flexible tails can adopt a brushlike conformation, increasing the total thickness of the layer.[32,33] Following this transition, the surface pressures increase sharply due to the resistance of the stiff paired aromatic cores, which eventually collapsed into bilayers by changing orientation from face-on to a vertical one.

The hydrophobic nature of the aromatic rod blocks and the hydrophilic nature of terminal PEO blocks drive the overall surface behavior of the molecules studied here and make it very similar to other rod−coil materials studied in our previous work.[5,8,13] However, the unique shape of these molecules with T-like rigid aromatic cores makes their structural reorganization very peculiar. Indeed, unlike other types of linear rod−coil molecules, T-shaped amphiphilic rod−coils form *paired, dimerlike* molecular packing with face-on orientation of these pairs at the air−water interface. Such close association is obviously caused by both strong, $\pi-\pi$ interactions of aromatic cores and steric limitations on their

(25) (a) Yang, W.; Chai, X.; Chi, L.; Liu, X.; Cao, Y.; Lu, R.; Jiang, Y.; Tang, X.; Fuchs, H.; Li, T. *Chem. Eur. J.* **1999**, *5*, 1144. (b) Ajayaghosh, A.; George, S. J. *J. Am. Chem. Soc.* **2001**, *123*, 5148. (c) Huang, X.; Li, C.; Jiang, S.; Wang, X.; Zhang, B.; Liu, M. *J. Am. Chem. Soc.* **2004**, *126*, 1322. (d) Guo, P.; Zhang, L.; Liu, M. *Adv. Mater.* **2006**, *18*, 177.

(26) 1375 cm^{-1} (CH_3 deformation), 1363 cm^{-1} (CH_2 wagging, C−C stretching), 1339 cm^{-1} (CH_2 wagging).

(27) Miyazawa, T.; Fukushima, K.; Ideguchi, Y. *J. Chem. Phys.* **1962**, *37*, 2764.

(28) Harder, P.; Grunze, M.; Dahint, R.; Whitesides, G. M.; Laibinis, P. E. *J. Phys. Chem. B* **1998**, *102*, 426.

(29) Cox, J. K.; Yu, K.; Constantine, B.; Eisenberg, A.; Lennox, R. B. *Langmuir* **1999**, *15*, 7714.

(30) The area of the aromatic rod (A_{aromatic}) approximates the limiting area of the molecule and stays constant during compression. Therefore, the area of PEO at a certain pressure ($A_{\text{PEO},\pi}$) can be calculated according to the pressure−area isotherm. The compression ratio of PEO chains is considered as the ratio of $A_{\text{PEO},\pi}$ to the area at the start of pressure elevation ($A_{\text{PEO},0}$). Finally, the effective contents of aromatic rod (W_{aromatic}'%) could be estimated as $W_{\text{aromatic}}'\% = 1/(A_{\text{PEO},\pi}/A_{\text{PEO},0} \times W_{\text{PEO}}\%/W_{\text{aromatic}}\% + 1)$.

(31) Xu, Z.; Holland, N. B.; Marchant, R. E. *Langmuir* **2001**, *17*, 377.

(32) (a) Karim, A.; Tsukruk, V. V.; Douglas, J. F.; Satija, S. K.; Fetters, L. J.; Reneker, D. H.; Foster, M. D. *J. Phys.* **1995**, *5*, 1441. (b) Luzinov, I.; Julthongpiput, D.; Malz, H.; Pionteck, J.; Tsukruk, V. V. *Macromolecules* **2000**, *33*, 1043.

(33) Halperin, A.; Tirrell, M.; Lodge, T. P. *Adv. Polym. Sci.* **1992**, *100*, 33.

packing under confined space conditions. Moreover, further reduction of the surface area available for these molecules initiate their assembly into *one-dimensional, chainlike, cylindrical aggregates* of paired molecules with several dozens of molecules in a single aggregate, a unique feature of the T-shaped molecules studied here and usually not observed for conventional, linear rod−coil amphiphilic molecules. In addition, this paired aggregation is so strong that it is preserved at the highest compression in the course of flipping and formation of vertically oriented cores. Such an association, and its "flip−flop" behavior within monolayers, can cause associated changes in optical and electrical properties that might be interesting for responsive surfaces and interfaces.

Acknowledgment. This work was supported by the National Creative Research Initiative Program. The BK21 program from the Ministry of Education and Human Resources Development and NSF funding DMR-0646958 are gratefully acknowledged. The authors thank Dr. Sergiy Peleshanko for technical assistance with LB measurements.

LA703660V